Chapter 2

Active nematics with quenched disorder

2.1 Introduction

Dynamics and steady-state of a collection of active self-propelled particles with different kinds of inhomogeneities has become an interesting area of research [Chepizhko et al. (2013); Das et al. (2018a); Maitra (2020); Morin et al. (2016); Reichhardt & Reichhardt (2016); Toner et al. (2018)]. Recent studies have mostly focused on the polar self-propelled particles in the presence of inhomogeneous agents/medium [(Dombrowski et al., 2004; Sanchez et al., 2012; Sumino et al., 2012)]. The effect of disorder in active polar particles introduces many exciting features, which, in general, do not present in the corresponding equilibrium system of the same symmetry [Imry & Ma (1975)]. Studies on the effect of disorder in apolar particles are limited to the equilibrium system only [Rotunno et al. (2005)]. Disorders are present almost everywhere inactive apolar systems [Reichhardt & Reichhardt (2017)], but ordering and steady-state of active apolar particles with the disorder is rarely studied.

Variety of systems where particles have head-tail symmetry, like vibrated granular rods [Blair et al. (2003); Sokolov et al. (2007)], collection of molecular motors, cytoskeletal

filaments [Cisneros et al. (2011); R. Kemkemer & Gruler (2000)], mesenchymal, epithelial cells monolayers [Blanch-Mercader et al. (2018); Duclos et al. (2017); Kawaguchi et al. (2017); Saw et al. (2017)], bacterial colonies [Dell'Arciprete et al. (2018); Doostmohammadi et al. (2016a); Yaman et al. (2019)], and colonies of swarming filamentous bacteria [Li et al. (2019)] are a few examples of the active apolar system. The collection of such active apolar particles, forming an orientationally ordered state, is called *active nematics*. Most of the previous active nematic studies are for a clean system [Bertin et al. (2009); Chaté et al. (2006); Doostmohammadi et al. (2018); Ramaswamy et al. (2003)]. But, inhomogeneity or disorder can play a crucial role in steady-state and kinetics of active nematics, which is our current study's focus.

In this chapter, we study quenched disorder's effect on a collection of active apolar particles on a two-dimensional substrate. The disorder is introduced as a random field of strength h_0 in the coarse-grained hydrodynamic equations of motion for slow variables; local density $\rho(\mathbf{r},t)$ and order parameter $\mathscr{Q}(\mathbf{r},t)$. We first characterize the steady-state and then study the ordering kinetics. We calculate the nematic order parameter (NOP) $\mathbf{Q}$ *vs.* system size N for different h_0. For clean or homogeneous active nematic, NOP decay algebraically with N (quasi-long range order, QLRO). But for a finite disorder, NOP shows a power-law decay, for small N and a disorder dependent crossover to an exponential decay (short-range order, SRO) for large N, and the same we confirm by the calculation of two-point orientation correlation function in the steady-state, using a linear approximation. The origin of such crossover for the finite disorder ($h_0 \neq 0$) is due to the pinning of the $\pm 1/2$ defects. For large enough N, it breaks the system in uncorrelated domains, and the size of these domains depends on the disorder strength. Although the orientation field is significantly affected due to disorder, the density fluctuation remains unaffected and shows the usual giant number fluctuation (GNF) [Chaté et al. (2006); Mishra & Ramaswamy (2006); Ramaswamy et al. (2003) for all disorder strengths (h_0).

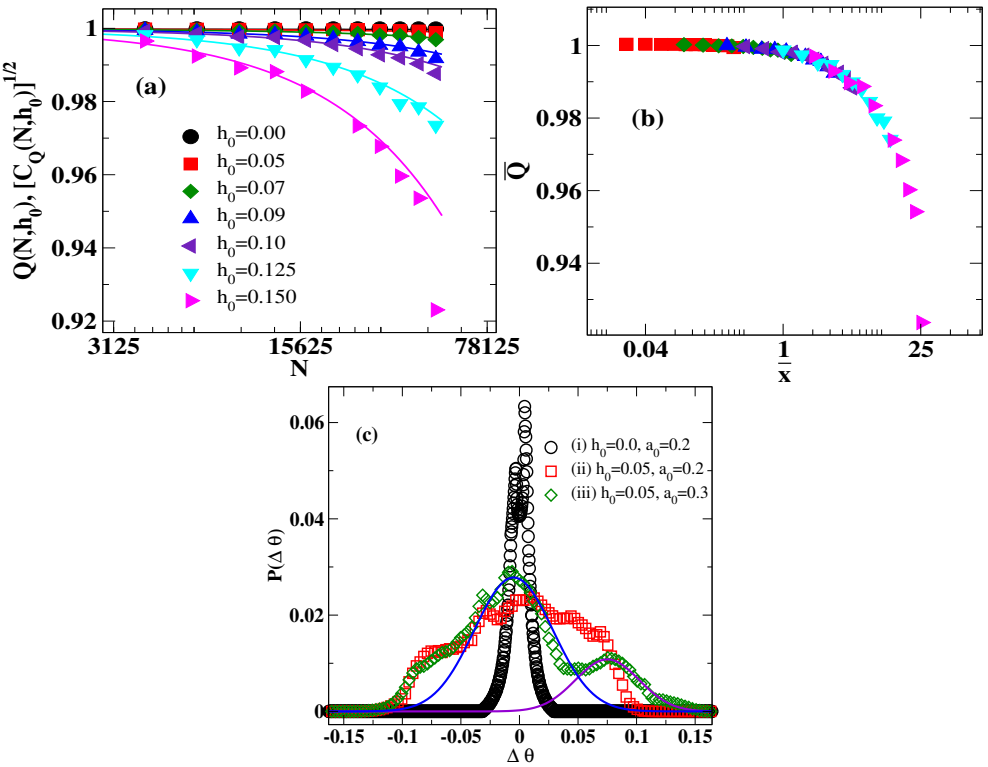

Fig. 2.1 (Color online) (a) NOP **Q** *vs.* system size $N = K \times K$ for different h_0 (symbols) and $\sqrt{C_{\mathscr{Q}}}$, Eq. (2.3) (solid lines), (b) Scaled NOP, $\bar{Q} = Q \times N^{\mathscr{B}'/2}$ *vs.* $\bar{x} = N \times {h_0}^4$. (c) Probability distribution function $P(\Delta\theta)$ of angle fluctuations of angular orientation for different values of (h_0, a_0) i.e. $(0.0, 0.2)$,$(0.05, 0.2)$ and $(0.05, 0.3)$. Data for $h_0 = 0.05$, $a_0 = 0.3$ (data points) fitted with Gaussian for two distinct peaks (solid lines).

We also studied the effect of disorder on the dynamics of the defects and the ordering kinetics. The *effective* dynamic growth exponent, z_{eff} [Bray (1994)] increases on increasing disorder. The two-point correlation functions for both fields show good dynamics scaling for all disorder, but no static scaling is found for different disorder.

We organize the paper as follows: we introduce the model of our system in Sec. 2.2. In Sec. 2.3, we discuss the steady-state properties, then we discuss defect dynamics and system kinetics in Sec. 2.4, further, in sec 2.5 we calculate the two-point correlation functions. We summarize the results in Sec. 2.7.

2.2 Model and Numerical details

We construct a monolayer of self-propelled apolar particles of length l, on a two-dimensional substrate of friction coefficient χ. Each particle is driven by an inherent driving force F acting along the particle's long axis. The ratio of the force F to the friction coefficient gives a constant self-propulsion speed $v_0 = F/\chi$ to each particle. The apolar nature of the particle makes them move forward and backward with *equal* probability with a step size equal to v_0. On a time scale, large compared to the interaction time and length scale much larger than the particle size, the dynamics of the system is governed by coupled hydrodynamic equations of motion for slow variables *viz.* local density $\rho(\mathbf{r},t)$, and local NOP $\mathscr{Q}(\mathbf{r},t)$ [de Gennes & Prost (1993)],

$$\partial_t \rho = a_0 \nabla_i \nabla_j \rho \mathscr{Q}_{ij} + D\rho\nabla^2\rho \tag{2.1}$$

$$\partial_t \mathscr{Q}_{ij} = [\alpha_1(\rho) - \alpha_2(\mathscr{Q} : \mathscr{Q})]\mathscr{Q}_{ij} + \beta(\nabla_i \nabla_j - \tfrac{1}{2}\delta_{ij}\nabla^2)\rho + D_{\mathscr{Q}}\nabla^2 \mathscr{Q}_{ij} + H_{ij} + \Omega_{ij} \tag{2.2}$$

The Eqs. (2.1) and (2.2) written in dimensionless units by rescaling all lengths by the length of the particle and time by the collision time and are of the same form as derived from the microscopic rule-based model in [Bertin et al. (2009)], with an additional term due to *quenched disorder*. The quenched disorder is introduced as *random field* in the free energy density $\mathscr{F} = -\mathscr{Q} : (\mathbf{hh} - \frac{\mathbf{I}}{2})$. Which further leads to $H_{ij} = (h_i h_j - h_0^2 \frac{1}{2}\delta_{ij})$, in equation 2.2, in two-dimensions $i, j = 1, 2$ are the spatial indices for the two components of vectors. Where, $h_i = h_0(cos\phi, sin\phi)$, here h_0 is the disorder strength and $\phi(\mathbf{r})$ is a uniform random angle between $(0, 2\pi)$, with mean zero, quenched in time (no time dependence) and space correlation $\langle \phi(\mathbf{r})\phi(\mathbf{r}')\rangle = \delta(\mathbf{r} - \mathbf{r}')$.

The last term, Ω_{ij} is a tensorial symmetric traceless white noise with mean zero, such that $\langle \Omega_{ij}(\mathbf{r}, t)\Omega_{kl}(\mathbf{r}', t')\rangle = \triangle_0 \delta(\mathbf{r} - \mathbf{r}')\delta(t - t')\varepsilon_{ijkl}$. Here, $\triangle_0$ is the noise strength and $\varepsilon_{ijkl} = \frac{1}{2}(\delta_{ik}\delta_{jl} + \delta_{il}\delta_{jk} - \delta_{ij}\delta_{kl})$.
In the above Eqs. 2.1 and 2.2 we keep the model minimal and ignore the flow field [Giomi et al. (2013)], completely; or assume the interaction among the particle is short range volume exclusion, and no hydrodynamic interaction. Hence the system we study is *dry* active nematics.

The random field introduced in our current model is similar to the random field in XY-model (RFXY-model) [Imry & Ma (1975)]. Hereafter we refer our model as random field active nematic (RFAN) when $h_0 \neq 0$, and clean-active nematic (clean-AN) for $h_0 = 0$.
To perform the numerical integration of Eqs. 2.1 and 2.2 we construct a two-dimensional $K \times K$ square lattice with periodic boundary condition (PBC) and discretise the space and

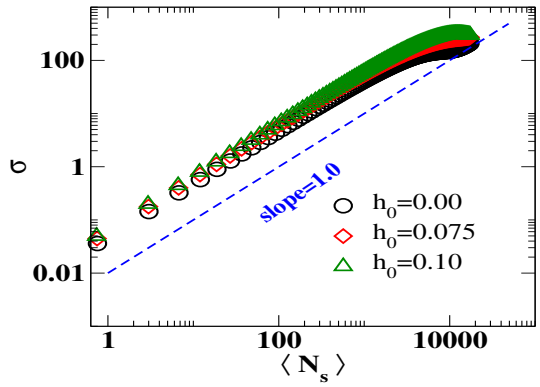

Fig. 2.2 (Color online) Number fluctuation σ *vs.* $< N_s >$ plot for different disorder strengths, and $K = 300$.

time derivatives using Euler scheme ($\Delta x = 1.0$ and $\Delta t = 0.1$). Initially, we start with random homogeneous density, with mean ($\rho_0 = 0.75$), and random orientation.

We first study the steady-state of the system for $h_0 = (0.0, 0.15)$ and system size, i.e. $K = 64\ to\ 512$. Coarsening is studied for larger $K = 1024$. Steady-state results are obtained for simulation time $t = \mathscr{O}(10^6)$ and the average over 10 independent realisations. One simulation time is counted after update of Eqs. 2.1 and 2.2 for all lattice points. Parameters in Eqs. (2.1) and (2.2) are ($a_0 = 0.1\ to\ 0.3$), $D_\rho = \frac{1}{4}(a_0^2 + 1)$, $\rho_0 = 0.75$, $\rho_c = 0.5$, $\alpha_2 = 1$, $\beta = 0.25$, *and* $D_{\mathscr{Q}} = 1$, $\triangle_0 = 10^{-4}$ and we check that, system remains stable for the chosen set of parameters.

2.3 Steady state properties

We first measure the steady-state properties of RFAN for different h_0. The global ordering in the system is measured by calculating the nematic order parameter (NOP) defined as $\mathbf{Q} = \langle \frac{1}{N} \sqrt{|\sum_{i=1}^{N} cos(2\theta_i)|^2 + |\sum_{i=1}^{N} sin(2\theta_i)|^2} \rangle$, where the sum runs over all the lattice points. $\langle .. \rangle$ shows the average over many realisations. We compare the measured $\mathbf{Q}$ in numerical simulation with the analytical expression for the two-point orientation correlation function

$C_{\mathscr{Q}}$ (Eq. 2.3), obtained from a linearised treatment of small fluctuation in a uniform ordered phase. We calculate the equal time Fourier transformed spatial correlation of angle, $S_{\mathbf{q}}(\theta)$ as a function of wavevector $\mathbf{q}$ and present our result for $q_x = q_y$. Starting from the equations of motion 2.1 and 2.2, a straight forward linearised approximation shows that for a finite disorder strength,

$$C_{\mathscr{Q}}(N) \simeq \frac{1}{N^{\mathscr{B}'}} e^{-\mathscr{C}' h_0^4 N} \tag{2.3}$$

which is obtained from the inverse Fourier transform of orientation structure factor $S_{\mathbf{q}}(\theta)$ at wave-number $q \simeq N^{-1/2}$. The coefficients in Eq (2.3), $\mathscr{B}' = 1.17 \times 10^{-4}$ and $\mathscr{C}' = 3.9 \times 10^{-3}$ (for $a_0 = 0.2$) are constants and depends on the system parameters. Hence $C_{\mathbf{Q}}$ is a product of algebraic and exponential decay with N. Fig. 2.1(a), data points shows the plot of NOP *vs.* N for different disorder strengths, h_0. For clean-AN, $\mathbf{Q}$ decays algebraically as N^{-B}, where $B \simeq 1.05 \times 10^{-4}$, depends on system parameters. Also, B is small, since, for the given parameters, clean-AN is in the deep ordered state and significantly away from the isotropic-nematic transition, where it shows the instability [Das et al. (2017); Shi & Ma (2010, 2013); Shi et al. (2014)]. For finite disorder, $\mathbf{Q}$ shows the deviation from the pure algebraic decay. It decays algebraically for small N and leads a crossover to exponential decay for a larger N. The larger the disorder strength, the crossover to exponential decay appears for smaller N.

In Fig. 2.1(a) lines are plot of $\sqrt{C_{\mathscr{Q}}(N, h_0)}$, Eq. (2.3). For clean-AN, $C_{\mathscr{Q}}(N, 0)$ is pure power-law whereas, for RFAN, it decays exponentially for higher N. Hence crossover happens after a disorder dependent N, $N_c(h_0) \sim h_0^{-4}$. We find a good match of lines (eq. 2.3) and data from the simulation. We see a systematic deviation between data points from the simulation

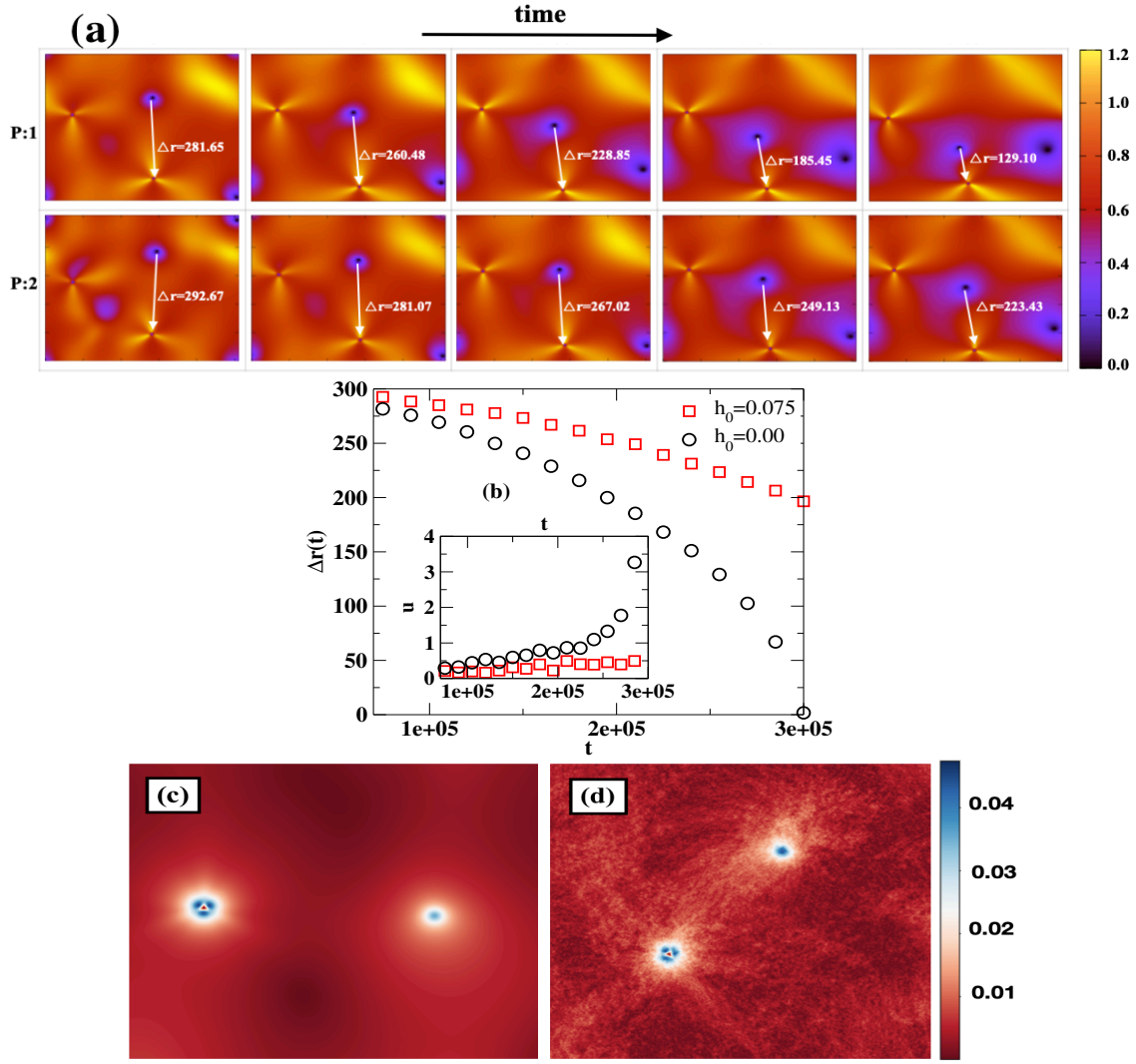

Fig. 2.3 (Color online) (a) Snapshots of local NOP $\mathscr{Q}$: upper panel (P:1) is for clean-AN (i.e. $h_0 = 0.0$) and bottom panel (P:2) is for RFAN ($h_0 = 0.075$) and the number along the white arrow is the relative separation $(\Delta r(t))$ between the $+$ and $-1/2$ defects. (b) $\Delta r(t)$ *vs.* t plot for $h_0 = 0.0, 0.075$. u is the relative speed of defects defined as $u = |\frac{d}{dt}\Delta r(t)| \times 10^{-3}$ and plotted in the inset of (b). (c) Snapshot of density current near the defects for clean-AN, $h_0 = 0.0$ and (d) RFAN, $h_0 = 0.075$. Intensity of colors shows the magnitude of the density current. Data is generated for system size $N = 512^2$.

and the linear study lines for large h_0, which is due to nonlinearities present in the model. In Fig. 2.1(b) we plot the $\mathbf{Q} \times N^{\mathscr{B}'/2}$ *vs.* $N \times h_0^4$ for different h_0 and find a good collapse of data for different disorder strengths.

To further understand the steady state in RFAN, we calculate the probability distribution function (PDF) $P(\Delta\theta)$ of angle fluctuations $\Delta\theta$ from the mean direction. Fig. 2.1(c) shows the plot of $P(\Delta\theta)$ *vs.* $\Delta\theta$ for different (h_0, a_0). $P(\Delta\theta)$ for clean-AN shows a very narrow peak at $\Delta\theta = 0$, whereas, for RFAN, PDF has a much broader distribution and more than one peak at non-zero $\Delta\theta$ (see Sec. 2.6 for snapshots). Lines in Fig. 2.1(c) are fit to two distinct peaks for $h_0 = 0.05, a_0 = 0.3$ with Gaussian. On increasing activity, the width of the distribution sharpens, and more distinct peaks emerge. Hence it infers the stronger intra-domain ordering and distinct ordered domains for large activity. Similarly, for a more considerable disorder, $P(\Delta\theta)$ shows a more number of such different peaks, which means that smaller domains emerge more if we further increase the disorder strength (data not shown).

In Sec. 2.6, we show the snapshots of local NOP for clean, $h_0 = 0.05$ and $h_0 = 0.1$, which shows that for a clean system, the final state is globally ordered, whereas, for RFAN, different ordered domains are formed and survived at late times.

We also calculate the steady-state density fluctuation, for all disorder, number fluctuation $\sigma = \sqrt{\langle {N_s}^2 \rangle - \langle N_s \rangle^2} \sim < N_s >$, where N_s is the mean number of particle in subcells, fig. 2.2, which shows a giant number fluctuation (GNF), as found in [Chaté et al. (2006); Mishra & Ramaswamy (2006); Ramaswamy et al. (2003)]. When compared with the linearised calculation of two-point density structure factor, as given in Eq. (2.36), for $q \simeq N^{-1/2}$, density fluctuation should show the fluctuations larger than the clean AN. But large fluctuation can arise for size $N_s > N_c \sim h_0^{-4}$, which is hard to achieve in numerical simulation. Hence in general, inhomogeneity does not affect the density fluctuations in active nematic, although it significantly changes the nature of two-point orientation correlation function. Now we further

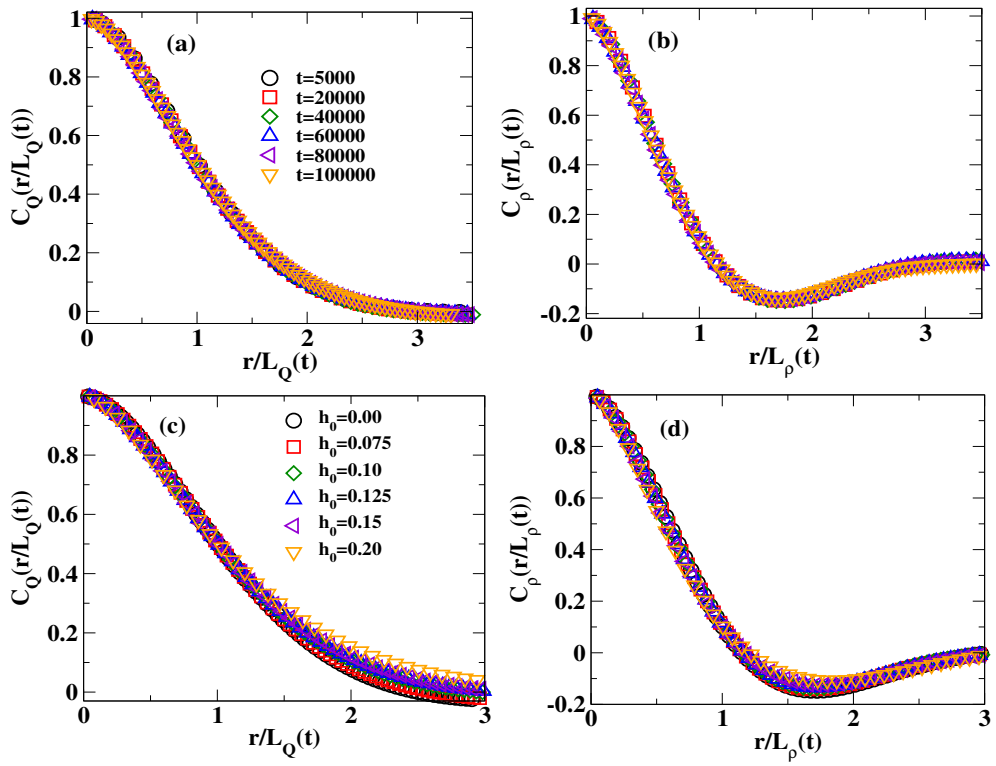

Fig. 2.4 (Color online) Two-point correlation function $C_{\mathscr{Q},\rho}$ *vs.* scaled distance $r/L_{\mathscr{Q},\rho}(t)$. (a-b) Two-point correlation function for RFAN i.e. $h_0 = 0.1$ at different simulation time (t). (c-d) Two-point correlation function for different h_0 and at fixed simulation time $t = 10^5$.

study the ordering kinetics to such steady-state.

2.4 Kinetics

2.4.1 Defect dynamics

When the system brought from a disordered state to an ordered state, ordering happens through the process of domain formation and which is due to the creation and annihilation of $\pm 1/2$ topological defects. In two-dimensional active nematics, these defects have topological geometry [Vromans & Giomi (2016)]. A $+1/2$ defect has a comet-like structure and moves

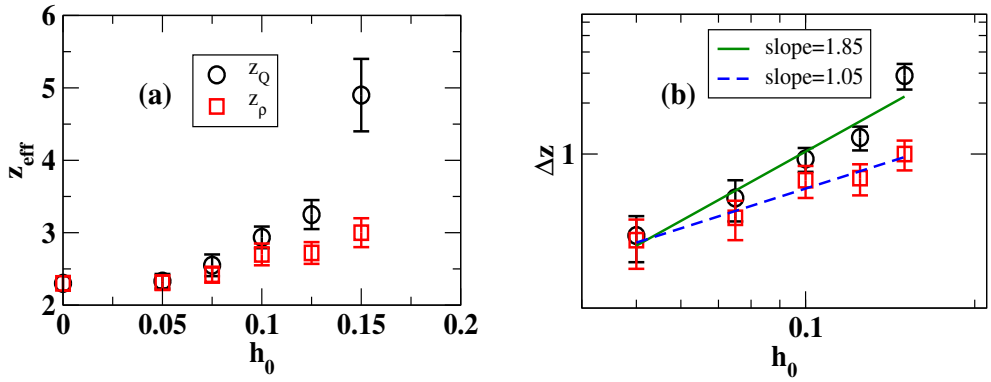

Fig. 2.5 (Color online) Plots of dynamic growth exponent $z_{eff}(h_0)$ *vs.* disorder strength h_0 (a), Δz vs. h_0 on log − log scale (b).

along the axis parallel to its tail, whereas a $-1/2$ defect has a three-fold symmetry and does not have any preferred direction of motion [Giomi et al. (2013); Mishra et al. (2014); Narayan et al. (2007)]. The dynamics of defects play a vital role in the ordering of the system [Bray (1994)]. In Fig. 2.3(a-b), we study the dynamics of defects for a clean-AN ($h_0 = 0.0$) as well for RFAN ($h_0 = 0.075$). Fig. 2.3(a) shows the snapshots of local NOP, $\mathscr{Q}$, for clean-AN (upper panel) and RFAN (lower panel). White arrows show the relative separation, $\Delta r(t)$, between a pair of $\pm 1/2$ defects. The arrow's tail and head represent the position of $+1/2$ and $-1/2$ defects, respectively. We see that the disorder slows the dynamics of the $+1/2$. The variation of $\Delta r(t)$ *vs. time* is shown in Fig. 2.3(b). The length of the white arrow in Fig. 2.3(a) decreases with time (or Δr decay with time Fig. 2.3(b)), which shows the two defects come close to each other. For clean-AN, $\Delta r(t)$ decay at a faster rate, whereas it takes a longer time in the presence of disorder. Hence the relative speed is small in the presence of disorder, as shown in the inset of Fig. 2.3(b). To further understand the mechanism of slowing down of defect dynamics, in Fig. 2.3(c-d), we show the snapshot of the local density current near a pair of $\pm 1/2$ defects. Density current $\mathbf{J}_\rho$ defined from Eq. (2.1), which can be rewritten as continuity equation, $\partial_t \rho = -\nabla \cdot \mathbf{J}_\rho$ where $\mathbf{J}_\rho = -a_0 \nabla \cdot (\rho \mathscr{Q}) - D_\rho \nabla \rho$. The intensity of colors shows the magnitude of the density current. For clean-AN, current flow is smooth near the defects Fig.

2.3(c), whereas with disorder ($h_0 = 0.075$), current flow is distorted, Fig. 2.3(d), which results in slower growth dynamics, we will discuss next. We also studied the effect of activity on the relative speed of a pair of defects. For larger activity, the relative separation (starting from the same relative separation) between a pair of defects decreases faster, and hence they annihilate quickly. Which, in turn, results in more ordering for the same disorder strength (see the Sec. 2.6 for details).

2.4.2 Growth law and scaling properties

As we discussed in previous paragraph, disorder affect the defect dynamics, and it can further influence the kinetics of domain ordering. We characterise the domain growth by calculating the correlation functions for orientation $\mathscr{Q}$, $C_{\mathscr{Q}}(\mathbf{r},t) = \langle \mathscr{Q}(\mathbf{0},t) : \mathscr{Q}(\mathbf{r},t) \rangle$ and, local density ρ, $C_{\rho}(\mathbf{r},t) = \langle \delta\rho(\mathbf{0},t)\delta\rho(\mathbf{r},t) \rangle$, where $\delta\rho(\mathbf{r},t) = \rho(\mathbf{r},t) - \rho_0$ is the deviation of the local density from the mean ρ_0. With time both correlations increases due to domain growth. Fig. 2.4(a-b) show the plot of $C_{\mathscr{Q}}(r/L(t))$ and $C_{\rho}(r/L(t))$ *vs.* scaled distance $r/L_{\mathscr{Q},\rho}(t)$ and they all collapse to a single curve. Where the characteristic length $L_{\mathscr{Q},\rho}(t)$ is calculated from the first zero crossing of $C_{\mathscr{Q}}(\mathbf{r},t))$ and $C_{\rho}(\mathbf{r},t)$. Fig. 2.4(c-d) shows the plot of $C_{\mathscr{Q}}(r/L_{\mathscr{Q}}(t))$ and $C_{\rho}(r/L_{\rho}(t))$ *vs.* scaled distance $r/L_{\mathscr{Q},\rho}(t)$ calculated at equal time ($t = 10^5$) for different disorder h_0. We find no scaling for different disorder strengths for both $\mathscr{Q}$ and ρ. Therefore, for all disorder strengths, the system shows good dynamic scaling but no static scaling in orientation and density.

The equilibrium analogue of clean-AN is XY-model and the characteristic length of growing domain in two-dimensional $XY-$model goes as $L_{XY}(t) \sim (t/\ln(t))^{1/2}$ [Bray (1994); Pargellis et al. (1992)]. Hence we assume that for RFAN, $L_{\mathscr{Q},\rho} \sim (t/\ln(t))^{1/z_{eff,\mathscr{Q},\rho}}$ and further calculate the dynamics growth exponent $z_{eff,\mathscr{Q},\rho}$ from correlation length $L_{\mathscr{Q},\rho}(t)$, defined as $\frac{1}{z_{eff,\mathscr{Q},\rho}} = \langle \frac{d\ln L_{\mathscr{Q},\rho}(t)}{d(t/\ln t)} \rangle$ [Bray (1994); Mishra et al. (2014); Pargellis et al. (1992); Yurke et al. (1993)],

where $\langle..\rangle$ is mean value of z_{eff} over intermediate time ($t \sim 1000\, to\, 15000$) when it remains constant for at least one decade, fig. 2.5(a). We find that $z_{eff,\mathscr{Q},\rho} \simeq 2$ for Clean-AN and increases on increasing h_0. In fig. 2.5(b), we plot the $\Delta z = z_{eff} - 2$ vs. h_0 on $\log - \log$ scale. The change Δz increases algebraically with h_0 with power ~ 2 and ~ 1 for $\mathscr{Q}$ and ρ respectively. Hence growth kinetics of density field shows small change in comparison to orientation field. Or small change in growth kinetics of density field affects the orientation field substantially.

2.4.3 Morphology of ordered domains

We study the effect of disorder on the morphology of ordering domains. We calculate the behaviour of scaled two-point correlation functions $C_{\mathscr{Q},\rho}(r/L_{\mathscr{Q},\rho})$ for small $r/L_{\mathscr{Q},\rho}$. In the limit of small $r/L_{\mathscr{Q},\rho}$, $C_{\mathscr{Q},\rho}(r/L_{\mathscr{Q},\rho}) \sim 1 - (\frac{r}{L_{\mathscr{Q},\rho}})^{\alpha}$, where α is called the cusp exponent and features the domain morphology [Bray (1994); Das & Barma (2000)]. In Fig. 2.6 we plot the $1 - C_{\mathscr{Q},\rho}(r/L_{\mathscr{Q},\rho})$ *vs.* scaled distance $r/L_{\mathscr{Q},\rho}$ on $\log - \log$ scale and estimate the cusp exponent α for both fields $(\mathscr{Q},\rho)$. The exponent, $\alpha \simeq 1.7$ for both fields and for all disorder strengths. Hence domain morphology remains unaffected in the presence of disorder.

2.5 Linearized hydrodynamic calculation of two-point correlation functions

We start with the hydrodynamic equations of motion for local density ρ and NOP $\mathscr{Q}$ as introduced in Eq. (2.1) and (2.2),

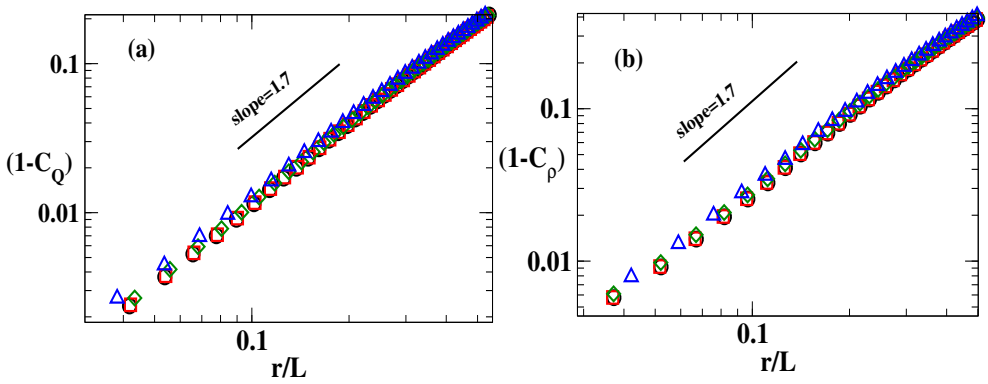

Fig. 2.6 (Color online) Cusp's exponent α (slope of the plot) for Q and ρ field. Different symbols used for different values of disorder strength: $h_0 = 0.0$ (circle), $h_0 = 0.05$ (square), $h_0 = 0.075$ (diamond), $h_0 = 0.10$ (triangle).

First, two terms on the R. H. S. of Eq. (2.2) are the mean-field terms: where, $\alpha_1(\rho) = \alpha_0(\frac{\rho}{\rho_c} - 1)$ where ρ_c is the critical density, where $\alpha_0 = 1$ is chosen as unity for simplicity. System shows homogeneous ordered state for $\alpha_1(\rho_0) > 0$, and disordered isotropic state when $\alpha_1(\rho_0) < 0$, where ρ_0 is the mean density of particles. The third term is coupling to the density field and the fourth term is the diffusion in $\mathscr{Q}$. Origin of such diffusion can be obtained from the equal elastic constant approximation of Frank-free energy for two-dimensional equilibrium nematic [Chaikin & Lubensky (1995); Gennes (1974)].

We rewrite Eqs. (2.1) and (2.2) neglecting the higher order fluctuations about the homogeneous ordered steady state. The local nematic order parameter $\mathscr{Q}$ is given as $\mathscr{Q} = \frac{S}{2}\begin{bmatrix} \cos 2\theta & \sin 2\theta \\ \sin 2\theta & -\cos 2\theta \end{bmatrix}$ where, S is a scalar and a measure of ordering. We define $\delta\rho$, δS and θ as the fluctuation terms from their mean values ρ_0, S_0 and θ_0 respectively. Here, $S_0 = \sqrt{\frac{2\alpha_1(\rho_0)}{\alpha_2}}$, and is obtained from (Eq. (2) main text) for homogeneous steady state.

Therefore, to linear order we have $\mathscr{Q}_{11} = \frac{1}{2}(S_0 + \delta S)$, $\mathscr{Q}_{12} = \theta S_0$, and (Eq. (1) main text) gives,

$$\partial_t(\rho_0+\delta\rho) = a_0[\partial_x{}^2(\rho_0+\delta\rho)\tfrac{(S_0+\delta S)}{2} + \partial_y{}^2(\rho_0+\delta\rho)\tfrac{(-(S_0+\delta S))}{2} + 2\partial_x\partial_y(\rho_0+\delta\rho)S_0\theta] + D_\rho\nabla^2(\rho_0+\delta\rho) \tag{2.4}$$

or,

$$\partial_t\delta\rho = a_0[(\partial_x^2\tfrac{(S_0\delta\rho+\rho_0\delta S)}{2} - \partial_y^2\tfrac{(S_0\delta\rho+\rho_0\delta S)}{2} + 2S_0\rho_0\partial_x\partial_y\theta] + D_\rho(\partial_x^2+\partial_y^2)\delta\rho \tag{2.5}$$

or,

$$\partial_t\delta\rho = (\tfrac{a_0S_0}{2}+D_\rho)\partial_x^2\delta\rho + (D_\rho - \tfrac{a_0S_0}{2})\partial_y^2\delta\rho + \tfrac{a_0\rho_0}{2}(\partial_x^2-\partial_y^2)\delta S + 2a_0\rho_0S_0\partial_x\partial_y\theta \tag{2.6}$$

while, the equation for δS (Eq. (2) main text) in homogeneous steady state gives,

$$0 = [\alpha_1(\rho_0) + \alpha_1{}'(\rho_0)\delta\rho - \tfrac{\alpha_2}{2}(S_0{}^2 + 2S_0\delta S)]\tfrac{S_0+\delta S}{2} + ... \tag{2.7}$$

also, $\alpha_1(\rho_0) - \frac{\alpha_2}{2}S_0{}^2 = 0$. Therefore we have,

$$(\alpha_1{}'(\rho_0)\delta\rho - \alpha_2S_0\delta S)(S_0+\delta S) = 0 \tag{2.8}$$

$$\delta S = \frac{\alpha_1^{'}(\rho_0)\delta\rho}{\alpha_2 S_0} \tag{2.9}$$

or,

$$\delta S = \Gamma\delta\rho \tag{2.10}$$

where, $\Gamma = \frac{\alpha_1^{'}(\rho_0)}{\alpha_2 S_0}$ and $\alpha_1^{'} = \frac{\partial\alpha_1(\rho)}{\partial\rho}|_{\rho=\rho_0}$. Hence, Eq. (2.6) can be re-written as,

$$\partial_t\delta\rho = (\tfrac{a_0 S_0}{2} + D_\rho)\partial_x^2\delta\rho + (D_\rho - \tfrac{a_0 S_0}{2})\partial_y^2\delta\rho + \tfrac{a_0\rho_0}{2}\Gamma(\partial_x^2 - \partial_y^2)\delta\rho + 2a_0\rho_0 S_0\partial_x\partial_y\theta \tag{2.11}$$

or,

$$\partial_t\delta\rho = (\tfrac{a_0 S_0}{2} + D_\rho + \Gamma\tfrac{a_0\rho_0}{2})\partial_x^2\delta\rho + (-\tfrac{a_0 S_0}{2} + D_\rho - \Gamma\tfrac{a_0\rho_0}{2})\partial_y^2\delta\rho + 2a_0\rho_0 S_0\partial_x\partial_y\theta \tag{2.12}$$

or,

$$\partial_t\delta\rho = K_1\partial_x^2\delta\rho + K_2\partial_y^2\delta\rho + K_3\partial_x\partial_y\theta \tag{2.13}$$

Where, $K_1 = (\frac{a_0 S_0}{2} + D_\rho + \Gamma\frac{a_0\rho_0}{2})$, $K_2 = (-\frac{a_0 S_0}{2} + D_\rho - \Gamma\frac{a_0\rho_0}{2})$ and $K_3 = 2a_0\rho_0 S_0$.

Now the equation of motion for $\mathscr{Q}_{12}$,

$$\partial_t \mathscr{Q}_{12} = [\alpha_1(\rho) - \alpha_2(\mathscr{Q}:\mathscr{Q})]\mathscr{Q}_{12} + \beta(\nabla_1\nabla_2 - \tfrac{1}{2}\delta_{12}\nabla^2)\rho + D_{\mathscr{Q}}\nabla^2\mathscr{Q}_{12} + H_{12} + \Omega_{12} \tag{2.14}$$

Here, $\mathscr{Q}_{12} = S_0\theta$ therefore, in linear order, $[\alpha_1(\rho) - \alpha_2(\mathscr{Q}:\mathscr{Q})]\mathscr{Q}_{12}$ will not survive. $h_1h_2 = {h_0}^2 cos\phi sin\phi = {h_0}^2\Phi(\mathbf{r})$, where $\Phi(\mathbf{r}) = cos\phi sin\phi$.

$$\partial_t\theta = \tfrac{\beta}{\rho_0 S_0}\partial_x\partial_y\delta\rho + D_{\mathscr{Q}}(\partial_x^2 + \partial_y^2)\theta + \tfrac{{h_0}^2}{\rho_0 S_0}\Phi + \tfrac{1}{\rho_0 S_0}\Omega \tag{2.15}$$

Taking the Fourier transform of equation (2.13) and (2.15), where Fourier modes are defined as, $f(\mathbf{q},\omega) = \int\int f(\mathbf{r},t)e^{i\mathbf{q}\cdot\mathbf{r}+i\omega t}d\mathbf{r}dt$, we get,

$$(K_1{q_x}^2 + K_2{q_y}^2 - i\omega)\delta\rho(\mathbf{q},\omega) + K_3 q_x q_y\theta(\mathbf{q},\omega) = 0 \tag{2.16}$$

and,

$$\tfrac{\beta}{\rho_0 S_0}q_x q_y\delta\rho(\mathbf{q},\omega) + [D_{\mathscr{Q}}({q_x}^2 + {q_y}^2) - i\omega]\theta(\mathbf{q},\omega) = \tfrac{{h_0}^2}{\rho S_0}\Phi(\mathbf{q}) + \tfrac{1}{\rho S_0}\tilde{\Omega}(\mathbf{q},\omega) \tag{2.17}$$

Solving equation (2.16) and (2.17) will give,

$$\mathbf{M}\begin{bmatrix}\delta\rho(\mathbf{q},\omega)\\ \theta(\mathbf{q},\omega)\end{bmatrix} = \frac{1}{\rho_0 S_0}\begin{bmatrix}0\\ {h_0}^2\Phi(\mathbf{q})+\tilde{\Omega}(\mathbf{q},\omega)\end{bmatrix} \tag{2.18}$$

where,

$$\mathbf{M} = \begin{bmatrix}K_1{q_x}^2+K_2{q_y}^2-i\omega & K_3 q_x q_y\\ \frac{\beta}{\rho_0 S_0}q_x q_y & D_{\mathscr{Q}}({q_x}^2+{q_y}^2)-i\omega\end{bmatrix} \tag{2.19}$$

by solving equation (2.18) for $q_x = q_y$, we get

$$\begin{bmatrix}\delta\rho(\mathbf{q},\omega)\\ \theta(\mathbf{q},\omega)\end{bmatrix} = \frac{1}{(D_1 q^4+\omega^2)-i\omega D_2 q^2}\begin{bmatrix}-K_3 q^2\\ 2D_\rho q^2-i\omega\end{bmatrix}\frac{({h_0}^2\Phi(\mathbf{q})+\tilde{\Omega}(\mathbf{q},\omega))}{\rho_0 S_0} \tag{2.20}$$

where, $D_1 = 4D_\rho D_{\mathscr{Q}} + 2a_0\beta$ and $D_2 = 2(D_\rho + D_{\mathscr{Q}})$. Equation (2.20) gives,

$$\delta\rho(\mathbf{q},\omega) = \frac{-K_3 q^2}{(D_1 q^4+\omega^2)-i\omega D_2 q^2}\frac{(h_0^2\Phi(\mathbf{q})+\tilde{\Omega}(\mathbf{q},\omega))}{\rho_0 S_0} \tag{2.21}$$

$$\theta(\mathbf{q},\omega) = \frac{2D_\rho q^2-i\omega}{(D_1 q^4+\omega^2)-i\omega D_2 q^2}\frac{(h_0^2\Phi(\mathbf{q})+\tilde{\Omega}(\mathbf{q},\omega))}{\rho_0 S_0} \tag{2.22}$$

Now, we first calculate the two point orientation correlation functions,

$$\langle\theta(\mathbf{q},\omega)\theta(-\mathbf{q},-\omega)\rangle = \frac{D_\rho{}^2 q^4+\omega^2}{(D_1 q^4+\omega^2)^2+\omega^2 D_2{}^2 q^4}\frac{[h_0^4\langle\Phi(\mathbf{q})\Phi(-\mathbf{q})\rangle+\langle\tilde{\Omega}(\mathbf{q},\omega)\tilde{\Omega}(-\mathbf{q},-\omega)\rangle]}{\rho_0 S_0} \tag{2.23}$$

here, $\langle\Phi(\mathbf{q})\Phi(-\mathbf{q})\rangle = \delta(\mathbf{q}+\mathbf{q})$ and $\langle\tilde{\Omega}(\mathbf{q},\omega)\tilde{\Omega}(-\mathbf{q},-\omega)\rangle = \triangle_0\delta(\mathbf{q}+\mathbf{q})\delta(\omega+\omega)$. Using this we get,

$$S_q(\theta) = \mathscr{C}(D_\rho, D_{\mathscr{Q}})\frac{h_0^4}{q^4} + \mathscr{B}(D_\rho, D_{\mathscr{Q}})\frac{1}{q^2} \tag{2.24}$$

Where, $\mathscr{C}(D_\rho, D_{\mathscr{Q}}) = \frac{4D_\rho{}^2}{\rho_0 S_0(4D_\rho D_{\mathscr{Q}}+2a_0\beta)^2}$ and $\mathscr{B}(D_\rho, D_{\mathscr{Q}}) = \frac{\pi\triangle_0}{2\rho_0 S_0}\frac{1}{c\sqrt{2(4b^2+c^2)}}[\frac{(2D_\rho{}^2+c(\sqrt{4b^2+c^2})-2b^2)}{\sqrt{c(c-\sqrt{4b^2+c^2})+2b^2}} + \frac{(-2D_\rho{}^2+c(\sqrt{4b^2+c^2})+2b^2)}{\sqrt{c(c+\sqrt{4b^2+c^2})+2b^2}}]$, where $b = \sqrt{2(2D_\rho D_{\mathscr{Q}}+a_0\beta)}$ *and* $c = \sqrt{2(D_\rho+D_{\mathscr{Q}})}$. Hence, the two point angle correlation function can be written as,

$$S_q(\theta) \simeq \frac{\mathscr{B}}{q^2} + \frac{\mathscr{C}h_0^4}{q^4} \tag{2.25}$$

Here, the coefficients $\mathscr{C}$ and $\mathscr{B}$ depends on system parameters.To get the two point correlation function for nematic orde parameter $C_{\mathscr{Q}}(x) \simeq exp(-G_\theta(x))$ [Chaikin & Lubensky

(1995)], where $G_\theta(x)$ is the inverse Fourier transform of $S_q(\theta)$ Eq. (2.25). Also, $G(x) = \mathscr{B}f(x) + \mathscr{C}h_0^4 g(x)$, where,

$$f(x) = \int_{2\pi/L}^{2\pi/a} \frac{d^2q}{4\pi^2} \frac{1-e^{i\mathbf{q}\cdot\mathbf{x}}}{q^2} \simeq ln(\Lambda|x|) \tag{2.26}$$

and,

$$g(x) = \int_{2\pi/a}^{2\pi/L} \frac{dq}{q^3} [\frac{1}{2} \int_0^{2\pi} d\theta (1 - e^{iq|x|cos\theta})] \tag{2.27}$$

or,

$$g(x) = \int_{2\pi/a}^{2\pi/L} \frac{dq}{q} (1 - J_0(q|x|) \tag{2.28}$$

here, J_n is the n^{th} order Bessel's function [Arfken & Weber (2012)].

$$g(x) = |x|^2 \int_0^1 \frac{du(1-J_0(u))}{u^3} + |x|^2 \int_1^{\Lambda|x|} \frac{du}{u^3} - |x|^2 \int_1^{\Lambda|x|} \frac{duJ_0(u))}{u^3} \tag{2.29}$$

$$g(x) = |x|^2 A + |x|^2 [-\frac{1}{2}(1 - \frac{1}{\Lambda^2|x|^2})] - |x|^2 \int_1^{2\pi/a|x|} \frac{duJ_0(u))}{u^3} \tag{2.30}$$

$$g(x) = |x|^2(A - \tfrac{1}{2} - |x|^2 \int_1^{2\pi/a|x|} \tfrac{duJ_0(u))}{u^3})$$

(2.31)

$$g(x) = \tfrac{a^2}{2\pi^2} + |x|^2(A - \tfrac{1}{2} - A')$$

(2.32)

here, $A = \int_{2\pi/L}^{2\pi/a} \frac{1-J_0(u)}{u^3} du \simeq 1.2$, $A' = \int_1^{2\pi/a|x|} \frac{J_0(u)}{u^3} du \simeq \int_0^{\infty} \frac{J_0(u)}{u^3} du \simeq 0.27$. Here, $a = 1$ is the lattice spacing.

$$g(x) = |x|^2 \times \mathscr{O}(0.01)$$

(2.33)

Hence, the orientation correlation function is given by,

$$C(x) \simeq \tfrac{1}{|x|^{\mathscr{B}}} e^{-|x|^2 \times \mathscr{O}(0.01) \times \mathscr{C} h_0^4}$$

(2.34)

when measured on the scale of system size $N = K^2$, we get,

$$C_{\mathscr{Q}}(N) \simeq \tfrac{1}{N^{\mathscr{B}'}} e^{-\mathscr{C}' h_0^4 N}$$

(2.35)

Here, $\mathscr{B}' = 1.17 \times 10^{-4}$ and $\mathscr{C}' = 3.9 \times 10^{-3}$.

Similarly, structure factor for density can be calculated using Eq. 2.21 and given by,

$$S_\rho(\mathbf{q}) = \gamma_1 \frac{h_0^4}{q^4} + \gamma_2 \frac{\triangle_0}{q^2} \tag{2.36}$$

where, $\gamma_1 = 0.5$ and $\gamma_2 = 0.4$ are constants and depends only on system parameters.

2.6 Snapshots for $\Delta\theta$ and NOP

2.6.1 Snapshots for $\Delta\theta$

The snapshots corresponding to Fig. 2.1 (c) is shown in Fig. 2.7. Here we can see that for a non-zero disorder in the system; distinct domains can be seen as the fluctuation in angular orientation $\Delta\theta$ represented by color bar varies significantly throughout the space whereas, for the clean system, the whole space is identical in terms of $\Delta\theta$. Also for larger activity $a_0 = 0.3$, the magnitude of $\Delta\theta$ fluctuations decreases, which confirms the stronger intra-domain ordering as found in $P(\Delta\theta)$.

2.6.2 Fixed a_0 and varying h_0

In fig 2.8, we show the snapshots for local NOP, $\mathscr{Q}$ at different simulation time for $a_0 = 0.2$ and different strengths of disorder in the system. We also included the multimedia files in the SM (see the supplementary materiel for the animations) for the same. We observe that as we increase the disorder in the system, dynamics of defect is slows down. Also for high disorder,

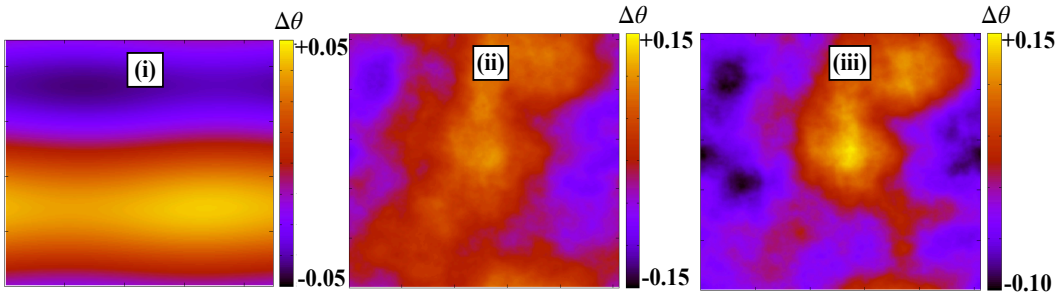

Fig. 2.7 (Color online) Snapshots of $\Delta\theta$ for $h_0 = 0.0, a_0 = 0.2$ (i), $h_0 = 0.05, a_0 = 0.2$ (ii) and $h_0 = 0.05, a_0 = 0.3$ (iii).

defects are pinned, which is responsible for formation of multiple smaller domains as shown in Fig. 2.1(c) and 2.7(i-iii).

2.6.3 Fixed disorder h_0 and varying activity a_0

Further, we change activity a_0 in equation (1) (main text), and plot the snapshots of local NOP, $\mathscr{Q}$ for fixed $h_0 = 0.05$ in fig 2.9 (see the supplementary materiel for animations). We find that, for a fixed h_0 ($= 0.05$ in this case), as we increase a_0, annihilation of defects happens faster than that of for the the smaller a_0. We also plot the relative separation $\Delta r(t)$ between a $+1/2$ and $-1/2$ defects *vs.* t in fig. 2.10(a) for three different $a_0 = 0.1$, 0.2 and 0.3. Also the relative speed, which is defined as, $u = |\frac{d}{dt}\Delta r(t)| \times 10^{-3}$, is plotted in fig 2.10(b).

2.7 Summary

We studied two-dimensional dry active nematics with the quenched random disorder using the the hydrodynamic equations of motion for the slow fields, *viz.* density ρ and orientation $\mathscr{Q}$, in a coarse-grained description.

The study from the numerical solution of equations of motion and the linearized hydrodynamic

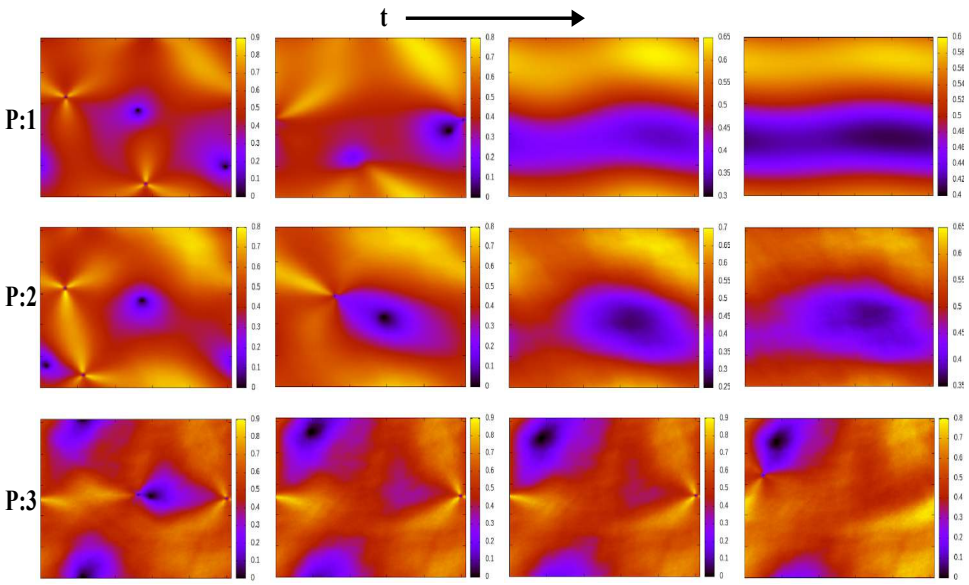

Fig. 2.8 (Color online) Snapshots of local NOP, $\mathscr{Q}$ for $a_0 = 0.2$ and for different disorder strength in the system. From top to bottom panel (P:1 to P:3) $h_0 = 0.0$, 0.05 and 0.1 respectively. Snapshots are generated at equal interval i.e. $t = 150000,\ 300000,\ 450000,\ and\ 600000$ from left to right respectively. Notice the numbers on the color bars.

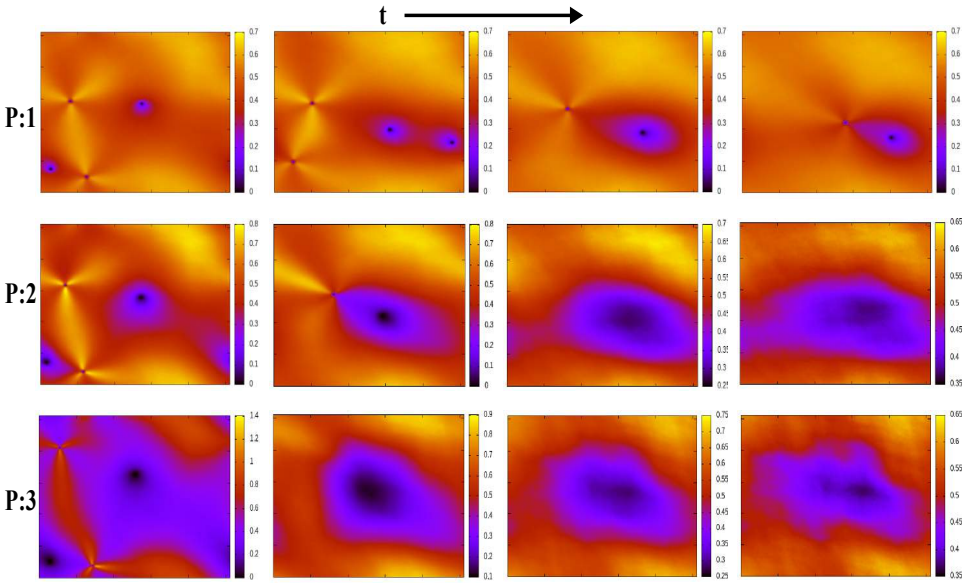

Fig. 2.9 (Color online) Snapshots of local NOP, $\mathscr{Q}$ for $h_0 = 0.05$ and for different activity in the system. From top to bottom panel (P:1 to P:3) $a_0 = 0.1$, 0.2 and 0.3 respectively. Snapshots are generated at equal interval i.e. $t = 150000,\ 300000,\ 450000,\ and\ 600000$ from left to right respectively. Notice the numbers on the color bars.

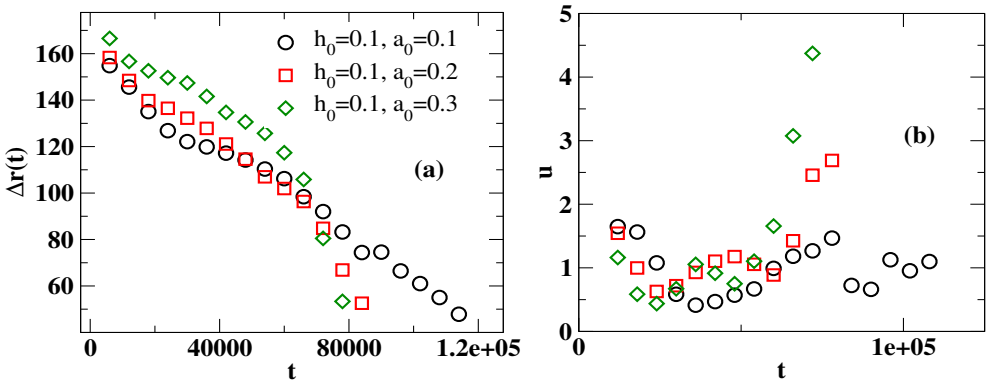

Fig. 2.10 (Color online) (a) Relative separation $\Delta(r)$ between $+1/2$ and $-1/2$ defects pair vs. time plot and (b) relative speed, $u = |\frac{d}{dt}\Delta r(t)| \times 10^{-3}$, of $\pm 1/2$ defects, for different value of a_0 and fixed $h_0 = 0.1$. t is the simulation time.

calculation shows that the orientation correlation follows a crossover from QLRO (algebraic decay of correlation) to SRO (exponential decay). Such crossover occurs due to the pinning of $\pm 1/2$ defects in the presence of finite disorder, which breaks the system in domains of different orientations. The size of such domains decreases on increasing disorder. For clean as well as RFAN, number fluctuation is giant.

We also studied the approach to the steady-state by (i) characterizing the dynamics of $\pm 1/2$ defects and (ii) calculation of the characteristic length of growing domains $L_{\mathscr{Q},\rho}(t)$. The slow dynamics of $+1/2$ defect leads to the slower domain growth in the presence of disorder. Although domain growth is slower in the presence of disorder, the two-point correlation function for both fields $C_{\rho,\mathscr{Q}}$ shows good dynamic scaling. Still, no static scaling is found for different disorder strengths. Domain morphology remains unaffected in the presence of disorder.

We find an interesting steady-state in RFAN, which is different from its corresponding equilibrium counterpart: random field XY-model [Imry & Ma (1975)]. Our study should motivate experimentalists to verify our findings and encourage us to study the effect of other kinds of disorders in active nematics. To make the model minimal, the effect of background fluid is ignored in our present study; hence it is for dry active nematic. It would be interesting to extend this study for wet active systems [Giomi et al. (2011, 2012, 2013).